Dynamics of Plastic Deformation Based on a Field Theory

S Yoshida, T Sasaki, G.A. Gaffney

Dynamics of Plastic Deformation Based on a Field Theory

S. Yoshida, T. Sasaki and G. A. Gaffney
Department of Chemistry and Physics, Southeastern Louisiana University,
SLU 10878, Hammond, LA 70402, USA, syoshida@selu.edu

ABSTRACT The dynamics of plastic deformation and fracture is formulated based on the field equation derived by physical mesomechanics, a recent gauge theory of deformation and fracture. A constitutive equation in plasticity has been derived from the field equation, and the dynamics associated with the transition from a late stage of plastic deformation to the fracturing stage is discussed. These concepts have been applied to an attempt to reveal the loading history of materials. Aluminum specimens have been preloaded with a tensile machine to different stress levels. After released from the preload, these specimens have been reloaded within the linear range of the loading curve, and the resultant displacement field has been analyzed with the use of in-plane sensitive electronic speckle pattern interferometry. Consequently, it has been found that through analysis of the interferometric fringe patterns it is possible to infer the stress level that the specimen has experienced under the preloading. The observed feathers in the fringe patterns have been explained via the above-mentioned constitutive equation and related dynamics.

Introduction

Structures and machines often fail after they pass periodic inspections, leading to catastrophic accidents. In particular, failure of aircrafts in normal flights happens even several hours after they pass the pre-flight inspection. In this type of incidence, it is usually the case that the inspection is conducted properly and the instrument used in the inspection is flawless. The prevailing inspection technology focuses on the detection of cracks at an early stage as possible. Recent advancement in the related technology such as ultrasonic technology allows the inspectors to detect micro-cracks. However, the procedure is time consuming, and moreover, it is not clear when a catastrophic accident occurs whether the inspection has failed to detect the micro-cracks that cause the failure or new cracks are generated after the inspection. Apparently, the problems at least partly come from the limitation of the theory that the inspection procedure is based on. The limitation of the current theory for accurate prediction of fracture is in most part due to the lack of solid physical foundation to connect the stages before and after micro-cracks appears. Conventional fracture mechanics [1] is quite successful in a number of applications, but it describes how a crack develops from its initial stage, and in addition, it basically relies on an elastic theory to formulate the fracturing process. If the crack generation can be predicted in an earlier stage, the inspection technology will drastically advance. It is definitely necessary to develop a theory that can describe the processes of deformation and fracture on the same foundation.

With this regard, a recent theory called physical mesomechanics [2] has a great potential. Based on one of the most fundamental principle in physics known as the gauge invariance [3, 4], this theory is capable of describing the dynamics of deformation universally. It is therefore possible to treat all the stages of deformation including fracture on the same theoretical foundation. A comprehensive description of physical mesomechanics can be found elsewhere [2]. In short, physical mesomechanics describes the plastic deformation as an energy dissipative process, where the elastic energy stored in solid-state materials is lost through dynamics of plasticity. Fracture is considered to be the final stage of deformation where the material becomes totally dissipative. In terms of kinematics, the dynamics can be described as a synergetic interaction between translational and rotational modes of displacement, where the temporal variation of the former alters the spatial variation of the latter, and vice versa. Formulaically, this dynamics is analogous to Maxwell's electrodynamics [3]. In fact, the physical mesomechanical field equation can be written in the same form as the Maxwell's equations, where the rate of translational displacement and the rotational displacement, respectively, correspond to the electric and magnetic field. Yoshida [5] has investigated on this similarity between the electromagnetic field and displacement filed in deforming object for the last 15 years, and recently has derived a constitutive equation in plasticity from the field equation [6].

In this study, an attempt is made to apply the translational-rotational dynamics of displacement field to reveal the hysteresis of deformation in aluminum specimen. Experiment has been conducted to analyze the responses of preloaded specimens to a low-level tensile load. The specimens were divided into four groups according to the stress level of preloading, *i.e*., from the preloading stress of the lowest level to the highest level, and after the preload was released, they were reloaded to the stress levels lower than the yield stress. The in-plane displacement of the reloaded specimens was examined with the use of an optical interferometric technique known as the Electronic Speckle Pattern Interferometry (ESPI) [7]. Consequently, the observations support our hypothesis that the loading history can be revealed, and in addition, the observed phenomena have been qualitatively explained *via* the above-mentioned translational-rotational dynamics.

Theoretical formulation

Physical mesomechanical field equation

The gauge theoretical formalism of physical mesomechanics can be conveniently understood as an extension of the global symmetry of the distortion tensor (matrix) in elasticity to local symmetry. In the theory of elasticity [8], the distortion tensor components, known as the normal/shear strain and rotation, are constant with respect to the space coordinates. The fact that the rotation tensor component is constant means that the material rotates as a rigid body, *i.e*., rotation is not deformation. In physical mesomechanics, the plastic deformation is characterized as the situation where the distortion tensor components are coordinate dependent [6]. Intuitively, this can be understood as follows. Imagine that a defect is generated inside a deforming material (Fig. 1). Naturally, the blocks around the defect will have the freedom of rotating differently; the rotation becomes coordinate dependent.

Fig. 1 Schematic views of material rotation due to external loading. Rigid body rotation (left) and four rotations around a defect at the center of the specimen (right).

Since the distortion tensor components contain spatial derivatives, this requires the replacement of the usual derivatives with covariant derivatives, or the introduction of a gauge term [3]. With the application of the Lagrangian formalism to the gauge field, this leads to the following Maxwell type field equation [4]. The general solution to this field equation is a decaying transverse wave of the translational and rotational displacement [9].

$$\nabla \cdot \vec{v} = j_o \tag{1}$$

$$\nabla \times \vec{\omega} = -\frac{1}{c}\frac{\partial \vec{v}}{\partial t} - \vec{J}\,, \tag{2}$$

where $\vec{v}$ is the velocity at (x, y, z), $\vec{\omega}$ is the angle of the local volume element from its rotational equilibrium, j_o and $\vec{J}$ are, respectively, the time and spatial components of the charge of symmetry, and c is the phase velocity of the displacement wave. $\vec{v}$ and $\vec{\omega}$ are connected as

$$\nabla \times \vec{v} = \frac{\partial \vec{\omega}}{\partial t}. \tag{3}$$

Dynamics of plastic deformation based on physical mesomechanics

Using the analogy to the Maxwell equations, we can rewrite eqs. (1) and (2) as below [6].

$$\nabla \cdot \vec{v} = \frac{\rho}{\varepsilon} \tag{4}$$

$$\nabla \times \vec{\omega} = -\varepsilon\mu\frac{\partial \vec{v}}{\partial t} - \vec{J}\,. \tag{5}$$

where ρ is the charge density, ε and $1/\mu$ are the density and the shear modulus of the medium. From the form $\rho = \varepsilon \nabla \cdot \vec{v}$, the charge density can be interpreted as the divergence of momentum density associated with strain concentration.

Application of divergence to eq. (5) with the use of eq. (4) leads to an equation of continuity.

$$\frac{\partial \rho}{\partial t} = -\frac{1}{\mu}(\nabla \cdot \vec{J}) . \tag{6}$$

With the interpretation that $\vec{J}/\mu$ represents the momentum loss associated with a flow of strain concentration (see below), this equation of continuity can be interpreted as the only way for the charge to change over time is the net momentum loss at the boundaries of the flow. Eq. (6) allows us to put

$$\frac{\vec{J}}{\mu} = \rho \vec{W}_d = \varepsilon(\nabla \cdot \vec{v})\vec{W}_d \tag{7}$$

where W_d is the drift velocity of the charge associated with ρ.

On the other hand, if the unit volume is subject to an external force in the direction of its velocity, the change in its momentum due to the force per unit time is

$$\frac{d\vec{p}}{dt} = \varepsilon(\nabla \cdot \vec{v})\vec{v} \tag{8}$$

This indicates that $\vec{J}/\mu$ is parallel to $\vec{v}$ and allows us to put

$$\frac{\vec{J}}{\mu} = \sigma \vec{v} \tag{9}$$

Comparison of eqs. (7) - (9) indicates that $\vec{J}/\mu$ is proportional to the change in the momentum over time, *i.e.*, effectively a longitudinal force acting on the unit volume. The quantity σ appearing in eq. (9) corresponds to the conductivity in electrodynamics. This is the cause of energy dissipation in plasticity.

Rearrangement of eq. (5) leads to

$$\varepsilon \frac{\partial \vec{v}}{\partial t} = -\frac{1}{\mu}(\nabla \times \vec{\omega}) - \frac{\vec{J}}{\mu} \tag{11}$$

Eq. (11) can be interpreted as the equation of motion acting on the unit volume, where the left-hand side represents the change in the momentum and the right-hand represents the external force. A recent study reveals that the first term on the right-hand side represent the recoverability mechanism in plasticity due to shear force associated with material rotation, and the second term is the energy dissipating force associated with the loss in momentum [6, 10]. Since eq. (11) holds under general conditions including when the left-hand side is zero leading to $\nabla \times \vec{\omega} = -\vec{J}$, it is possible to interpret that current flows along the boundary of rotations.

Plastic deformation and fracture criteria

From the gauge theoretical viewpoint that the plastic deformation is characterized as the situation where the distortion component is coordinate dependent, it is possible to interpret that when the rotation $\vec{\omega}$ is spatial dependent on the left-hand side of eq. (2), the condition for plastic deformation is satisfied. Indeed, by setting the left-hand side to zero, eq. (2) reduces to the elastic wave equation. Thus, the plastic deformation criterion can be given as

$$\nabla \times \vec{\omega} \neq 0 . \quad (12)$$

Condition (12) basically indicates that if different regions of a material rotate differently, the deformation is plastic, as oppose to that if the entire region of the material experiences a common rotation, the deformation is elastic.

Similarly, the fracture can be interpreted as the final stage of plastic deformation where the material loses its recoverability mechanism via the first term of the right-hand side of eq. (11). The difference from elastic deformation, where $\nabla \times \vec{\omega}$ is also zero, is that the current $\vec{J}$ is nonzero, causing the energy dissipation. Thus the fracture criterion [11] can be given as

$$\nabla \times \vec{\omega} = 0 \quad (13)$$

$$\frac{\vec{J}}{\mu} = \varepsilon(\nabla \cdot \vec{v}) W_d \neq 0 . \quad (14)$$

These indicate that if $\vec{\omega}$ and $\nabla \cdot \vec{v}$ can be monitored, it is possible to diagnose the current status of an object whether it is plastically deforming or in the fracturing stage. The idea we demonstrate in this study is that we monitor these quantities via the interferometric fringe patterns that represent the displacement filed of a deforming object.

Experiment

Displacement measurement with Electronic Speckle-pattern Interferometry (ESPI)

Fig. 2 illustrates the experimental arrangement used in this study. A dual beam type ESPI setup sensitive to in-plane displacement was arranged in front of an aluminum specimen attached to a tensile machine. A continuous wave, helium neon laser oscillating at 632.8 nm was used for the light source of the interferometer. The laser beam was split into two paths in a horizontal plane, and the resultant two beams configured as the two interferometric arms illuminate the surface of the specimen at the same angle of incidence so that the in-plane sensitivity was in the direction of the tensile axis. The CCD camera captured the image of the specimen at a constant interval of 0.04 – 0.1 s. The captured images were recorded into computer memory, where each image was subtracted from the image captured at a later frame, typically 10 – 20 frames later, so that an appropriate number of interferometric fringes were formed.

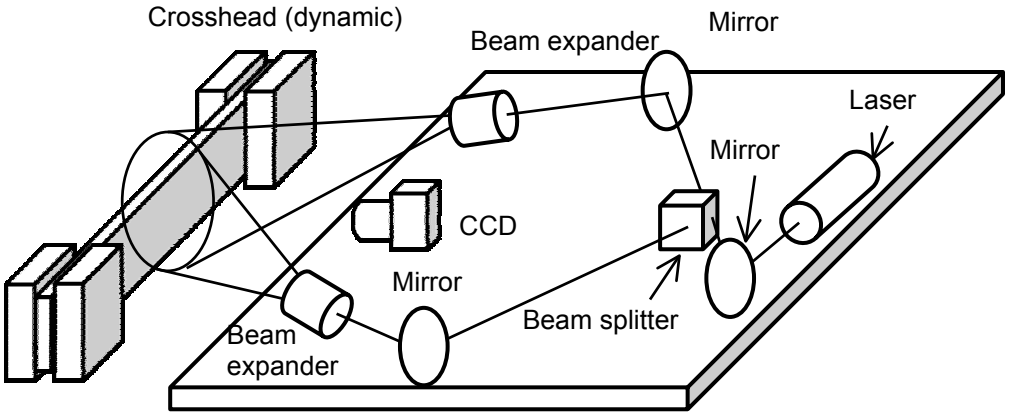

Fig. 2 Experimental arrangement

Preload and reload test

The specimen used in this study was 100 mm long, 20 mm wide and 0.5 mm thick pure aluminum with shallow notches at the center of the 100 mm sides. The tensile load was applied at a constant head speed of 20 μm/sec. Fig. 3 shows the loading characteristics of this aluminum specimen when it was pulled until fracture at 20 μm/sec (full load). These aluminum specimens were preloaded to four different stress levels of 85 kgf (Specimen A), 100 kgf (Specimen B), 106 kgf (Specimen C), and 109 kgf (Specimen D). All these specimens were reloaded to 80 kgf

for five times, with the ESPI setup turned on to capture the images. The four preload levels are indicated in Fig. 3 along with reloading characteristics of the four specimens. Note that the maximum reload level of 80 kgf is within the linear range of the loading characteristics observed when the specimen was pulled until fracture.

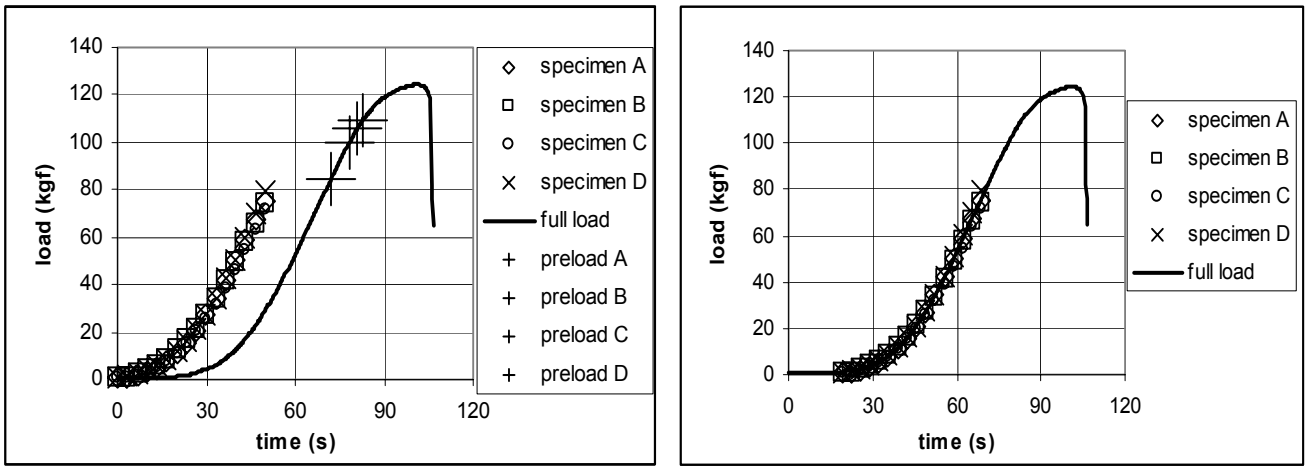

Fig. 3 Loading characteristics of full load and reloads. The reload characteristics are shifted on the right figure so that rising slopes can be compared with the full load characteristics.

Results and discussions

To facilitate the discussion regarding the fringe patterns in connection with the displacement field of the examined specimen, let's first consider general pattern of fringes. Refer to Fig. 4 and consider the fringes observed with an ESPI setup sensitive to horizontal displacement. When the specimen experiences horizontal stretch to the right, for example, the right end of the specimen displaces the most largely, the left end displaces the least and the rest parts displace in proportion to the distance from the right end. Consequently, the fringe pattern consists of vertical straight lines. If the deformation is uniform, the vertical lines are equally spaced. On the other hand, when the specimen experiences either pure shear deformation or rigid body rotation, the fringe pattern observed in the same ESPI setup consists of horizontal straight lines. If the deformation is a combination of these, which is normally the case, the resultant fringes are mixture of these patterns.

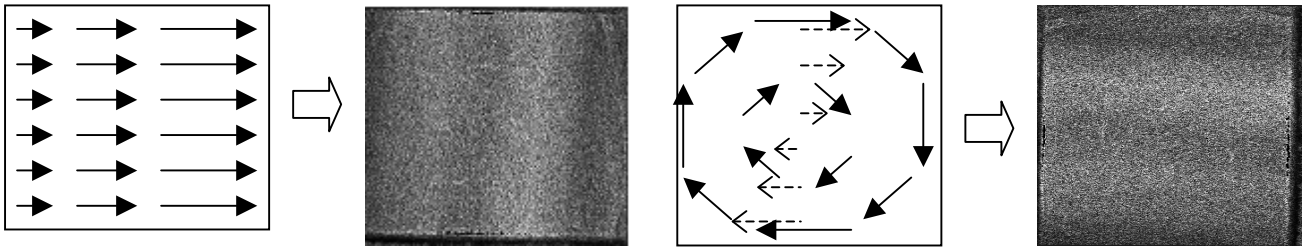

Fig.4 Fringe patterns representing uniform stretch (left), and pure shear deformation or rotation (right). The dashed lines in the right picture denote the horizontal components of the displacement under pure rotation, which a horizontally sensitive interferometer is sensitive to.

When reloaded, the preloaded specimens generally show the following trends as the applied load was increased from 0 kgf to 80 kgf.

Stage 1: The fringe patterns are random, often no fringes are observed.
Stage 2: The fringe patterns consist of horizontal wavy lines.
Stage 3: The fringe patterns consist of horizontal straight lines.
Stage 4: The horizontal lines observed in Stage 3 rotate upright. As the load increases, the lines keep rotating.
Stage 5: The fringes stop rotating and become mostly vertical.

The left image of Fig. 5 shows typical fringe patterns observed in third – fifth reloads in Specimen A – D when the reload level is around 10 kgf. The fringe patterns seen in top two rows (in Specimens A and B) are typical wavy fringes observed in Stage 2. The fringes seen in the two right columns in the third row are straight fringes observed in "Stage 3". The fringes seen in the bottom row are upright-rotating fringes observed in "Stage 4". Notice that in Specimen C (third row), the horizontal fringes are becoming more straight as the number of reload increases, indicating the transition from "Stage 2" to Stage "3" takes place as the reloading repeats. From this viewpoint, the leftmost pattern in the third row is an intermediate pattern between the stage 2 wavy and stage 3 straight fringes. Similarly, the right image of Fig. 5 shows typical fringes observed in the same reloads as the left image around the higher reload level of 50 kgf. The fringe patterns seen in this figure are basically upright-rotating fringes in Stage 4. Notice that in all rows the fringes become more upright as going from the left to right. This indicates that as the reloading repeats, the specimen experiences transition toward Stage 5.

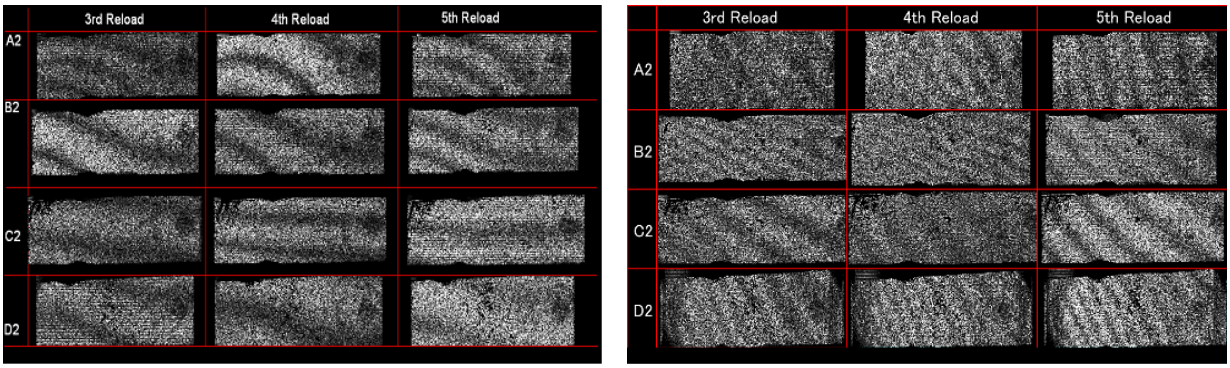

Fig.5 Fringe patterns observed with reload level of 10 kgf (left) and 50 kgf (right)

Considering the basic patterns in fringes shown in Fig. 4, and the plastic deformation and fracture criteria represented by eqs. (12) and (13), the wavy and straight fringes observed in Stage 2 and 3 can be interpreted as follows. The straight horizontal fringes in Stage 3 represents the fact that the deformation is characterized by a single rotation, or $\nabla\times\vec{\omega}=0$, *i.e.* the fracture criterion is satisfied. The material has already lost the recoverability represented by $\nabla\times\vec{\omega}/\mu$ [the first term on the right- hand side of eq. (11)]. In Stage 2, on the other hand, the horizontal fringes are wavy because the deformation is characterized by multiple rotations, or $\nabla\times\vec{\omega}\neq 0$ *i.e.* the material can still exert the recovery force represented by $\nabla\times\vec{\omega}/\mu$. Thus the transition from Stage 2 to Stage 3 can be interpreted as representing the process in which the material loses its recoverability associated with spatially dependent rotation represented by $\nabla\times\vec{\omega}\neq 0$.

The change in the fringe pattern from Stage 3 to Stage 5 through Stage 4 can be interpreted as follows. As the material loses the recovery force $\nabla\times\vec{\omega}/\mu$, the second term in eq. (11) [$\vec{J}/\mu$] becomes the dominant mechanism to resist the external force. In the present experimental condition, since the tensile machine exerts the load in the horizontal (x) direction, the material's net resisting force is in the x direction. On the other hand, the x-component of the two forces represented by the right-hand side of eq. (11) can be written, respectively, as

$$\frac{1}{\mu}(\nabla\times\vec{\omega})_x=\frac{1}{\mu}\frac{\partial\omega_z}{\partial y}=\frac{1}{\mu}\left(\frac{\partial^2 v}{\partial x\partial y}-\frac{\partial^2 u}{\partial^2 y}\right) \tag{15}$$

$$\left(\frac{\vec{J}}{\mu}\right)_x=\varepsilon(\nabla\cdot\vec{v})W_d=\varepsilon\left(\frac{\partial u}{\partial x}+\frac{\partial v}{\partial y}\right)W_d \tag{16}$$

The horizontally sensitive ESPI setup records the horizontal component of the displacement u. Thus the fringe patterns represent the terms containing u in eqs. (15) and (16). Therefore, the transition that the dissipation term $\vec{J}/\mu$ becomes dominant over the recovery force $\nabla\times\vec{\omega}/\mu$ should be seen as $\partial u/\partial x$ [the first term in the parenthesis of eq. (16)] dominates over $\partial^2 u/\partial y^2$ [the second term in the parenthesis of eq. (15)]. In other words

the x dependence of u dominates the y dependence of u. In the fringe patterns, this is observed as the horizontal fringes ($\partial u/\partial y >> \partial u/\partial x$) turning vertical fringes ($\partial u/\partial x >> \partial u/\partial y$). In this fashion, the fringes become mostly vertical in Stage 5.

Interestingly, the load levels at which these stages are observed vary among specimens depending on the level of the preload and the number of reloading. Generally speaking, the higher the preloading level or the number of reloading, the specimen tends to experience the respective stages at lower reload levels. Fig. 6 and 7 summarize the trend. The following observations are found.

Observation 1:
As the reloading is repeated, the transitions from Stage 1 toward stage 5 take place at lower reload levels.

Observation 2:
The above trend is more prominent in Specimens A and B than Specimens C and D. In particular, the reload level that causes the transition from Stage 2 to Stage 3 reduces remarkably from the first to second reloading in Specimen A and B.

Observation 3:
In all reloads, Specimen A and B show similar trends and Specimens C and D show similar trends, respectively. However, trends observed in both groups are different from each other.

Observation 4:
Specimens C and B barely show Stage 2 fringes, indicating that when this sample is preloaded to the level of 106 kgf or higher, the fracture criterion is almost satisfied so that the material barely exerts the recovery force from the beginning of reloads.

Observation 5:
In the first reload, Specimens A and B show Stage 2 pattern till the end of reload (80 kgf). In the second reload and after, they show Stage 3 pattern. This strongly indicates that the Specimen A and B experience fatigue in the first reload, and that the effect caused by the mechanism of fatigue is similar to the effect caused by the tensile load.

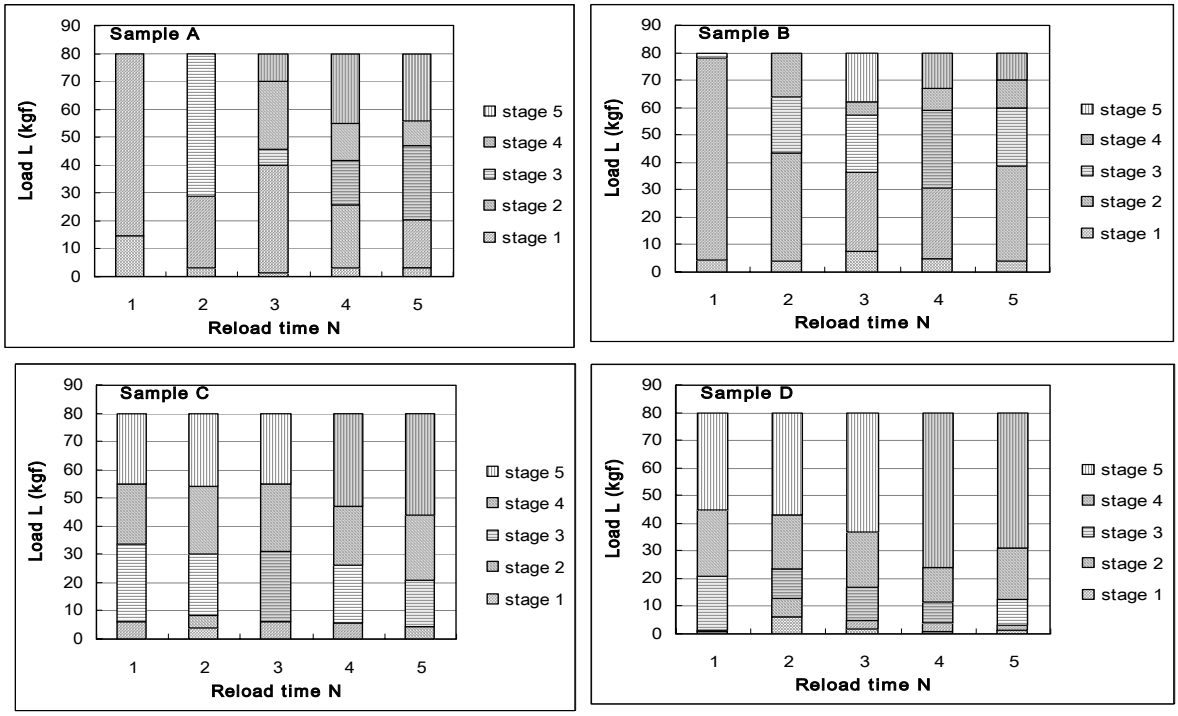

Fig. 6 Change in fringe patterns as reloading number increases.

Notice that whereas the above observations and the features observed in the fringe patterns enable us to infer the preload level, Fig. 3 indicates that the specimens preloaded to different levels show very similar reloading characteristics. This indicates that for the purpose of revealing loading history, it is necessary to analyze the spatial distribution of the displacement as seen in the fringe patterns. The loading characteristic, being representing the total displacement, does not have information to reveal the loading history.

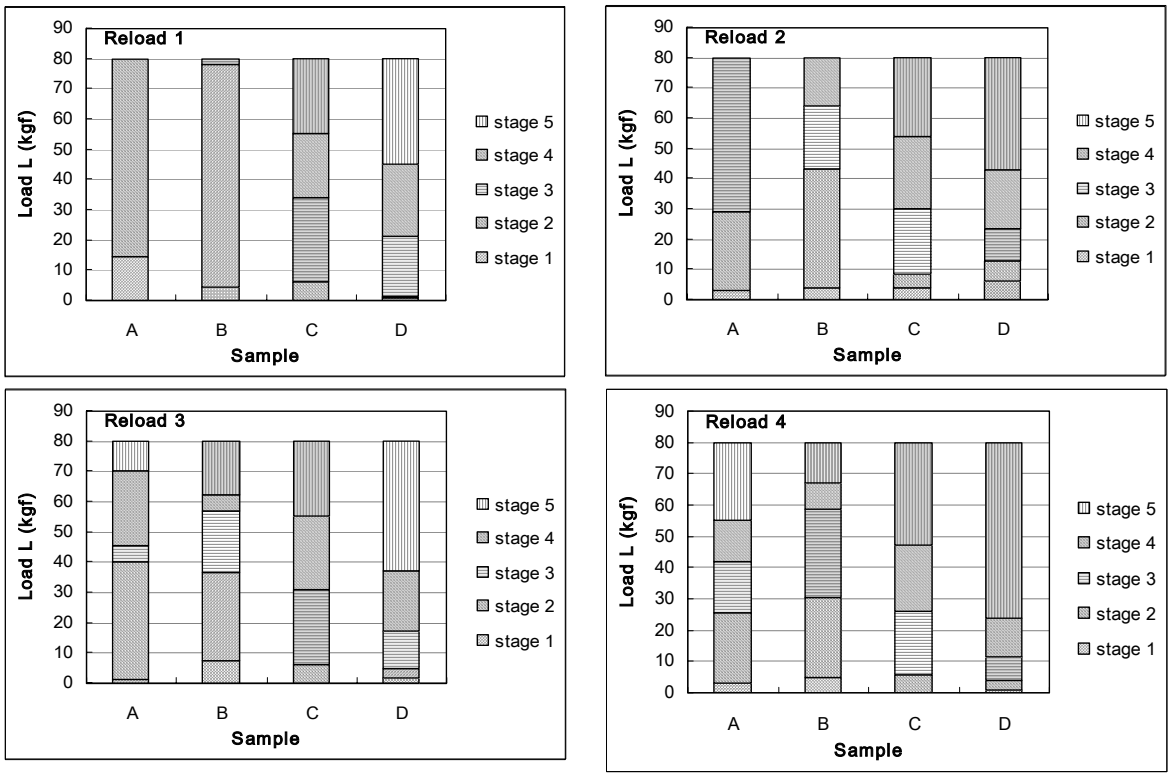

Fig. 7 Change in fringe patterns as preload level increases for each reload.

Conclusion

In summary, the dynamics of plastic deformation has been discussed based on the formalism originally developed by physical mesomechanics. The fracture is formulated as the final stage of deformation where the material becomes totally dissipative. The constitutive equation of plasticity derived from the physical mesomechanical field equation has been discussed in connection with the transitional stage from plastic deformation to fracture. These concepts have been applied to an attempt of revealing the loading history of aluminum specimens. The specimens have been preloaded to four different stress levels, and after the released from the preload, they are reloaded within the linear range of the loading characteristics. The change in the displacement field observed in the reloaded specimens has been analyzed with the use of an in-plane sensitive, electronic speckle pattern interferometric setup. It has been found that through analysis of the observed fringe patterns, it is possible to differentiate the preloaded specimens one from another according to the preload conditions. The observed features of the fringe patterns have been explained in accordance with the derived constitutive equation and related dynamics.

References

1. A. S. Tetelman and A. J. McEvily, Jr., *Fracture of Structural Materials*, John Wiley & Sons, Inc, New York (1967)
2. V. E. Panin ed., *Physical Mesomechanics of Heterogeneous Media and Computer-Aided Design of Materials*, vol. 1, Cambridge International Science, Cambridge (1998)

3. I. J. R. Aitchson and A. J. G. Hey, *Gauge theories in particle physics*, IOP Publishing, Ltd., Bristol and Philadelphia (1989)
4. V. E. Egorushkin, “Dynamics of plastic deformation: waves of localized plastic deformation in solids”, Rus. Phys., 35, 4, 316-334 (1992)
5. S. Yoshida, “Interpretation of mesomechanical behaviors of plastic deformation based on analogy to Maxwell electromagnetic theory”, Phys. Mesomech. 4, 3, 29-34 (2001)
6. S. Yoshida, “Dynamics of plastic deformation based on restoring and energy dissipative mechanisms in plasticity”, Phys. Mesomech. 11, 140-146 (2008)
7. R. S. Sirohi, Ed. *Speckle Metrology*, Marcel Dekker, Inc., New York (1993)
8. L. D. Landau and E. M. Lifshitz, *Theory of Elasticity*, 3rd ed., Course of Theoretical Physics, vol. 7, Butterworth-Heinemann, Oxford (1986)
9. S. Yoshida, “Observation of plastic deformation wave in a tensile-loaded aluminum-alloy”, Phys. Lett. A, 251, 54-60 (1999)
10. S. Yoshida, G. A. Gaffney, C. W. Schneider and R. L. Rourks, “Field Theoretical Approach to Deformation and Fracture”, Proc. SEM XI International Congress, June 2-5, Orlando, FL USA, 144-149 (2008)
11. S. Yoshida, “Consideration on fracture of solid-state materials”, Phys. Lett. A, 270, 320-325. (2000)